Inorganic Chemistry

Article

pubs.acs.org/IC

Two-Dimensional 3d–4f Heterometallic Coordination Polymers: Syntheses, Crystal Structures, and Magnetic Properties of Six New Co(II)–Ln(III) Compounds

Pau Díaz-Gallifa,[†] Oscar Fabelo,*[,‡,§] Jorge Pasán,[†] Laura Cañadillas-Delgado,[∇] Francesc Lloret,[⊥] Miguel Julve,[⊥] and Catalina Ruiz-Pérez*[,†]

[†]Laboratorio de Rayos X y Materiales Moleculares (MATMOL), Departamento de Física, Facultad de Ciencias, Universidad de La Laguna Avenida Astrofísico Francisco Sánchez s/n, E-38204 La Laguna, Tenerife, Spain

[‡]Institut Laue-Langevin, 71 avenue des Martyrs, C.S.20156, 38042, Grenoble, Cedex 9, France

[§]Instituto de Ciencia de Materiales de Aragón, CSIC-Universidad de Zaragoza C/Pedro Cerbuna 12, 50009 Zaragoza, Spain

[∇]Centro Universitario de la Defensa de Zaragoza Ctra, Huesca s/n, 50090 Zaragoza, Spain

[⊥]Departament de Química Inorgànica/Instituto de Ciencia Molecular (ICMol), Facultat de Química, Universitat de València C/Catedrático José Beltrán 2, E-46980 Paterna (València), Spain

Supporting Information

ABSTRACT: Six new heterometallic cobalt(II)-lanthanide(III) complexes of formulas $[Ln(bta)(H_2O)_2]_2[Co(H_2O)_6]\cdot 10H_2O$ [Ln = Nd(III) (**1**) and Eu(III) (**2**)] and $[Ln_2Co(bta)_2(H_2O)_8]_n\cdot 6nH_2O$ [Ln = Eu(III) (**3**), Sm(III) (**4**), Gd(III) (**5**), and Tb(III) (**6**)] (H_4bta = 1,2,4,5-benzenetretracaboxylic acid) have been synthesized and characterized via single-crystal X-ray diffraction. **1** and **2** are isostructural compounds with a structure composed of anionic layers of $[Ln(bta)(H_2O)_2]_n^{n-}$ sandwiching mononuclear $[Co(H_2O)_6]^{2+}$ cations plus crystallization water molecules, which are interlinked by electrostatic forces and hydrogen bonds, leading to a supramolecular three-dimensional network. **3**–**6** are also isostructural compounds, and their structure consists of neutral layers of formula $[Ln_2Co(bta)_2(H_2O)_8]_n$ and crystallization water molecules, which are connected through hydrogen bonds to afford a supramolecular three-dimensional network. Heterometallic chains formed by the regular alternation of two nine-coordinate lanthanide(III) polyhedra $[Ln(III)O_9]$ and one compressed cobalt(II) octahedron $[Co(II)O_6]$ along the crystallographic *c*-axis are cross-linked by bta ligands within each layer of **3**–**6**. Magnetic susceptibility measurements on polycrystalline samples for **3**–**6** have been carried out in the temperature range of 2.0–300 K. The magnetic behavior of these types of Ln(III)–Co(II) complexes, which have been modeled by using matrix dagonalization techniques, reveals the lack of magnetic coupling for **3** and **4**, and the occurrence of weak antiferromagnetic interactions within the Gd(III)–Gd(III) (**5**) and Tb(III)–Tb(III) (**6**) dinuclear units through the exchange pathway provided by the double oxo(carboxylate) and double syn–syn carboxylate bridges.

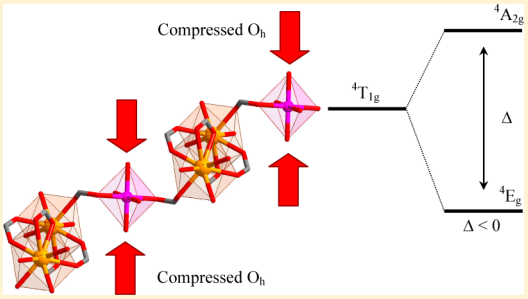

INTRODUCTION

The chemistry of metal-organic compounds has raised a great interest during the last decades.[1,2] The variety of properties of the coordination polymers make them good targets in research fields, such as magnetism, luminescence, catalysis, etc.[3]

From the magnetic point of view, the coordination polymers add new properties to those of the classical magnets (e.g., low density, electrical insulation, low-temperature fabrication, etc.). Among the first-row transition metal ions incorporated in the magnetic coordination polymers, the six-coordinate cobalt(II) ion is especially appealing, because of its anisotropic character and the three unpaired electrons that it has.[4] As far as the introduction of trivalent rare-earth cations in these compounds is concerned, some of the 4f elements bring large high anisotropic magnetic moments to the material, although the shielding effects generally produce weak magnetic interactions.

Unexpected magnetic properties in polynuclear compounds have been achieved by means of the combination of different spin carriers within the same molecular entity.[5] In particular, heterometallic 3d–4f assemblies have been the subject of intensive research by different groups, because of the diversity of their magnetic behavior.[6]

The rational assembly of the 3d and 4f ions is a more complicated task than dealing with the preparation of homometallic systems.[7] As it is well-known, a suitable choice of the ligand allows the bottom-up approach for extended networks (coordination polymers) through the connections between the polydentate ligands and metal centers. The initial preparative works about the mixed 3d–4f systems used

Received: April 11, 2014
Published: June 5, 2014

dx.doi.org/10.1021/ic5008582 | *Inorg. Chem.* 2014, 53, 6299–6308

polydentate Schiff-base ligands to perform the selective complexation of the two metal ions[8] and more recently, oxamidate-type ligands were employed to do the same.[9] All these ligands have in common the fact that they are mixed-donor linkers. The results obtained indicate that the oxophilic lanthanoid centers efficiently compete with the 3d metal ions for the O-donors, whereas the reverse is observed for the N-donors.[8,9] More recent studies have shown that the 3d−4f extended networks can be achieved with ligands being exclusively O-donors.[5c,10,11] Our approach will involve the use of the 1,2,4,5-benzenetetracarboxylic acid (H_4tba), which has the ability to combine the rigidity with a surprising high number of coordination modes toward Co(II)[12] and Ln(III)[13] ions in homometallic phases.

The hydrothermal method is the most extended synthetic route used to design 3d−4f compounds with mixed ligands. The previous preparative attempts that we have carried out to obtain heterometallic compounds have shown that the slow diffusion techniques constitute an excellent alternative method.[5c,10] In this respect, we have previously synthesized 3d−4f metal-organic frameworks involving the use of the gel growth;[5c,10] therefore, in the present work, we explore this alternative together with other slow reaction synthesis. We present here the syntheses and crystal structure of six new heteronuclear 3d−4f complexes of formulas $[Ln(bta)(H_2O)_2]_2\cdot[Co(H_2O)_6]\cdot 10H_2O$ [Ln = Nd(III) (**1**) and Eu(III) (**2**)] and $[Ln_2Co(bta)_2(H_2O)_8]_n\cdot 6nH_2O$ [Ln = Eu(III) (**3**), Sm(III) (**4**), Gd(III) (**5**), and Tb(III) (**6**)] together with the variable-temperature magnetic study of **3**−**6**.

EXPERIMENTAL SECTION

Materials and Methods. Reagents and solvents used in the syntheses were purchased from commercial sources and used without further purification. Elemental analyses (C, H, N) were performed with a Model EA 1108 CHNS/0 automatic analyzer.

Preparation of the Complexes. *General Procedure.* X-ray-quality crystals of compounds **1**, **2**, **3**, and **5** were grown by slow evaporation of aqueous solutions, whereas those of **4** and **6** have been obtained through the silica gel technique described by Henisch.[14]

The crystal growth of this series of complexes is not favored neither kinetically nor thermodinamically, and only a specific concentration of the reactants yields the heterometallic product. Therefore, two strategies have been selected to obtain these materials: the gel technique and the slow evaporation method.

The gel method lets us test a number of concentrations of the reactants in a single experiment; the concentration of the ligand is always the same, and those of the metal ions are constantly varying during the experience (according to their diffusion through the gel). However, collecting the crystals from the gel is a difficult task, specially when several phases grow simultaneously. Fortunately, in the cases of **4** and **6**, the crystals appeared in the gel interphase, simplifying their collection.

The solution method is simpler and the collection is easier; however, obtaining the correct values for the concentration of the reactants is much more difficult. We found that the lanthanide salts react immediately with the bta ligand to form the homometallic phase; the cobalt(II) salt, however, needs time to form a complex with the bta. Therefore, we selected a Co:Ln molar ratio of 20:1, to avoid the rapid formation of the homometallic Ln(bta) phase. Then, two scenarios arise. In the case of **1** and **2**, the crystals of the heterometallic phase appear simultaneously with those of the Ln(bta) phase, and, once collected, they have to be separated mechanically. In the case of **3** and **5**, the crystals that grow first are those of the heterometallic phases, which are removed from the solution to displace the equilibrium to the formation of these complexes.

All our attempts to grow single crystals with the remaining 4f elements by using these techniques were unsuccessful, and only the homometallic lanthanoid complex was obtained.

*Synthesis of $[Ln(bta)(H_2O)_2]_2[Co(H_2O)_6]\cdot 10H_2O$ [Ln = Nd (**1**) and Eu (**2**)].* An aqueous solution of 0.5 M NaOH was added dropwise to another aqueous solution (50 cm^3) of H_4bta (0.254 g, 1 mmol) until a pH value of ca. 5.0 was reached. Then, an aqueous solution (30 cm^3) of cobalt(II) nitrate hexahydrate (0.582 g, 2 mmol) and either neodymium(III) nitrate hexahydrate (0.044 g, 0.1 mmol) (**1**) or europium(III) nitrate pentahydrate (0.043 g, 0.1 mmol) (**2**) was added to the previous solution under vigorous stirring. The resulting pink solution was allowed to evaporate at room temperature. Pale pink needles of **1** and **2**, together with the corresponding homometallic phases, appeared after 2 days. They were mechanically separated, washed several times with a 50:50 (v/v) water/methanol solution, and air-dried. The yields are 22% and 31% for **1** and **2**, respectively, based on the starting amount of the lanthanide. Anal. Calcd for $C_{20}H_{44}CoNd_2O_{36}$ (**1**): C, 19.88%; H, 3.65%. Found: C, 19.89%; H, 3.67%. Anal. Calcd for $C_{20}H_{44}CoEu_2O_{36}$ (**2**): C, 19.63%; H, 3.61%. Found: C, 19.64%; H, 3.63%.

*Synthesis of $[Ln_2Co(bta)_2(H_2O)_8]_n\cdot 6nH_2O$ [Ln = Eu (**3**) and Gd (**5**)].* Compounds **3** and **5** were obtained following a procedure similar to that used for **1** and **2**, but using sodium carbonate (0.208 g, 2 mmol) instead of sodium hydroxide to neutralize the solution. Pale pink prisms of **3** and **5** were formed after a week of standing at room temperature. The solution was frequently looked at in order to collect the heterometallic phase before the precipitation of the homometallic phases. They were mechanically separated, washed with a 50:50 (v/v) water/methanol solution, and air-dried. The yields are 42% (**3**) and 35% (**5**). Anal. Calcd for $C_{20}H_{32}CoEu_2O_{30}$ (**3**): C, 21.53%; H, 2.89%. Found: C, 21.64%; H, 3.06%. Anal. Calcd for $C_{20}H_{32}CoGd_2O_{30}$ (**5**): C, 21.31%; H, 2.87%. Found: C, 21.32%; H, 2.81%.

*Synthesis of $[Ln_2Co(bta)_2(H_2O)_8]\cdot 6H_2O$ [Ln = Sm (**4**) and Tb (**6**)].* An aqueous solution of 0.5 M NaOH was added dropwise to an aqueous solution (10 cm^3) of H_4bta (0.127 g, 0.5 mmol) until a pH value of ca. 4.3 was reached. Then, tetramethoxysilane (1 cm^3) was added dropwise to the previous solution under vigorous stirring. The resultant clear solution was added to a test tube and stored at room temperature. After 2 days, the gel was set and an aqueous solution (3 cm^3) containing cobalt(II) nitrate hexahydrate (0.585 g, 1 mmol) and either samarium(III) nitrate hexahydrate (0.044 g, 0.1 mmol) (**4**) or terbium(III) nitrate pentahydrate (0.043 g, 0.1 mmol) (**6**) was carefully layered on the gel. Pale pink prisms of **4** and **6** were formed in the gel/solution interface after standing for a week at room temperature. They were mechanically separated, washed with a water/methanol (50:50 v/v) mixture, and air-dried. The values of the yield are of 25% (**4**) and 55% (**6**). Anal. Calcd for $C_{20}H_{32}CoSm_2O_{30}$ (**4**): C, 21.59%; H, 2.90%. Found: C, 21.64%; H, 3.12%. Anal. Calcd for $C_{20}H_{32}CoTb_2O_{30}$ (**6**): C, 21.26%; H, 2.86%. Found: C, 21.34%; H, 2.87%.

Physical Measurements. Magnetic susceptibility measurements on polycrystalline samples of compounds **3**−**6** were carried out in the temperature range of 2.0−300 K with a Quantum Design SQUID magnetometer under applied magnetic fields of 1 T (50 K < $T \leq$ 300 K) and 250 G ($T \leq$ 50 K). The magnetization measurements were performed at 2.0 K in the field range of 0−5 T. The values of the experimental magnetic susceptibility data were corrected for the diamagnetic contribution of the constituent atoms, as well as for the magnetization of the sample holder.

Crystal Structure Determination and Refinement. Single-crystal X-ray diffraction data sets were collected at 293 K (**1** and **3**−**6**) on a Nonius Kappa CCD diffractometer with graphite-monochromated Mo Kα radiation (λ = 0.71073 Å), while those of **2** were collected at 100 K at the ESRF synchrotron BM16 beamline (Grenoble, France), using λ = 0.7256 Å. Data were indexed, integrated, and scaled using the EVALCCD[15] (**1**, **3**−**6**) and HKL2000[16] (**2**) programs. It deserves to be noted that equivalent reflections were merged during the integration process using the HKL2000 program.[16] The structures of **1**−**6** were solved by direct methods and subsequent Fourier syntheses using the SHELXS97

dx.doi.org/10.1021/ic5008582 | Inorg. Chem. 2014, 53, 6299−6308

Table 1. Crystal Data and Details of the Structure Determination for Complexes 1−6

	1	2	3	4	5	6
formula	$C_{20}H_{44}CoNd_2O_{36}$	$C_{20}H_{44}CoEu_2O_{36}$	$C_{20}H_{32}CoEu_2O_{30}$	$C_{20}H_{32}CoSm_2O_{30}$	$C_{20}H_{32}CoGd_2O_{30}$	$C_{20}H_{32}CoTb_2O_{30}$
M	1207.96	1223.40	1115.31	1111.96	1125.89	1129.10
crystal system	monoclinic	monoclinic	triclinic	triclinic	triclinic	triclinic
space group	$P2_1/n$	$P2_1/n$	$P\bar{1}$	$P\bar{1}$	$P\bar{1}$	$P\bar{1}$
a (Å)	15.2410(9)	15.159(3)	8.5563(2)	8.5800(5)	8.5403(4)	8.5233(6)
b (Å)	8.7110(3)	8.666 (2)	8.8685(1)	8.8986(6)	8.8537(6)	8.8297(6)
c (Å)	15.7880(10)	15.744(3)	11.7221(2)	11.7367(7)	11.7225(5)	11.7246(5)
α (deg)	90.0	90.0	85.451(3)	85.428(5)	85.439(3)	85.427(4)
β (deg)	104.621(3)	104.80(3)	88.012(3)	87.998(6)	87.941(3)	87.955(4)
γ (deg)	90.0	90.0	63.791(3)	63.632(5)	63.764(3)	63.941(5)
V (Å^3)	2028.2(2)	1999.6(7)	795.53(3)	800.31(9)	792.54(7)	790.15(9)
Z	2	2	1	1	1	1
index ranges						
h	$-20 < h < 16$	$-0 < h < 20$	$-11 < h < 11$	$-12 < h < 12$	$-11 < h < 11$	$-11 < h < 9$
k	$-10 < k < 11$	$-0 < k < 11$	$-11 < k < 11$	$-12 < k < 12$	$-11 < k < 11$	$-11 < k < 10$
l	$-12 < l < 21$	$-21 < l < 20$	$-15 < l < 15$	$-16 < l < 16$	$-15 < l < 15$	$-14 < l < 15$
T (K)	293(2)	100(2)	293(2)	293(2)	293(2)	293(2)
ρ_{calc} (Mg m^{-3})	1.926	2.032	2.328	2.274	2.359	2.339
λ, Mo Kα (Å)	0.710 73	0.725 60	0.710 73	0.710 73	0.710 73	0.710 73
μ, Mo Kα (mm^{-1})	3.034	3.624	4.530	4.251	4.774	5.065
R_1, $I > 2\sigma(I)$ (all)	0.0572 (0.0888)	0.0658 (0.0821)	0.0281 (0.0360)	0.0287 (0.0366)	0.0248 (0.0289)	0.0381 (0.0520)
wR_2, $I > 2\sigma(I)$ (all)	0.1579 (0.1795)	0.2012 (0.2159)	0.0621 (0.0643)	0.0633 (0.0656)	0.0604 (0.0620)	0.0820 (0.0879)
total number of reflections	13 789	4857	13 412	16 572	13 871	7115
independent reflections, R_{int}	5093 (0.049)	4857 (0)	3640 (0.036)	4654 (0.0338)	3619 (0.030)	3426 (0.034)
goodness-of-fit, GOF	1.104	1.055	1.058	1.088	1.121	1.081

program.[17] All non-hydrogen atoms were refined anisotropically by full-matrix least-squares technique based on F^2, using the SHELXL97 program.[17] The hydrogen atoms of the bta^{4-} ligand have been set on geometrical positions and refined with a riding model. Those of the water molecules were neither found nor set. Crystallographic data for the structures of **1**−**6** have been deposited at the Cambridge Crystallographic Data Centre with CCDC reference numbers 984260, 984261, 984262, 984263, 984264, and 984265 for **1**, **2**, **3**, **4**, **5**, and **6**, respectively. The final geometrical calculations and the graphical manipulations were carried out with the PLATON[18] and DIAMOND[19] programs. A summary of the crystal data and refinement conditions is listed in Table 1 (**1**−**6**), whereas intermolecular contacts, selected bond lengths and angles are shown in the Supporting Information (Tables S1 and S2 for 1 and 2 and Tables S3 and S4 in 3−6).

RESULTS AND DISCUSSION

Structural Description. *$[Ln(bta)(H_2O)_2]_2[Co(H_2O)_6]\cdot 10H_2O$ [Ln = Nd (1) and Eu(2)].* **1** and **2** are isostructural compounds whose crystal structure consists of anionic layers of formula $[Ln(bta)(H_2O)_2]_n^{n-}$, mononuclear $[Co(H_2O)_6]^{2+}$ cations and crystallization water molecules, which are interlinked by hydrogen bonds, leading to a supramolecular three-dimensional network (see Figure 1 and Table S1 in the Supporting Information). A regular alternation of anionic layers and mononuclear cations occurs in **1** and **2**. Within each anionic layer, the lanthanide(III) ions form chains along the crystallographic b-axis, which are connected through the skeleton of the bta^{4-} ligand [see Figure 2 (left)]. Within each chain, two similar oxo(carboxylate) bridges are regularly alternated [O(2) and O(2)$^{(a-1)}$ between Ln(1) and Ln(1)$^{(a-1)}$ and O(7)$^{(b-1)}$ and O(7)$^{(c-1)}$ between Ln(1) and Ln(1)$^{(d-1)}$; symmetry code: $(a-1) = 1-x, 2-y, 2-z$; $(b-1) = 0.5-x, 0.5+y, 1.5-z$; $(c-1) = 0.5+x, 2.5-y, 0.5+z$; and $(d-1) = 1-x, 3-y, 2-z$] [see Figure 2 (right)]. The shortest intrachain metal−metal separations are 4.4073(4) (**1**) Å/4.3838(8) Å (**2**) [Ln(1)···Ln(1)$^{(a-1)}$] and 4.3772(4) (**1**) Å/4.3548(8) Å (**2**) [Ln(1)···Ln(1)$^{(d-1)}$] with values of the angle at the bridgehead oxo(carboxylate) atom of 117.6(2)° (**1**)/118.3(2)° (**2**) [Ln(1)−O(2)−Ln(1)$^{(a-1)}$] and 115.6(2)° (**1**)/116.0(2)° (**2**) [Ln(1)−O(7)$^{(b-1)}$−Ln(1)$^{(d-1)}$]. The values of the interlayer lanthanide···lanthanide distance [12.2783(6) Å (**1**) and 12.244(3) Å (**2**) for Ln(1)···Ln(1)$^{(e-1)}$; $(e-1) = 0.5+x, 2.5-y, -0.5+z$] are much greater than those between adjacent chains within each layer [9.4878(5) Å (**1**) and 9.430(4) Å (**2**) for Ln(1)···Ln(1)$^{(c-1)}$].

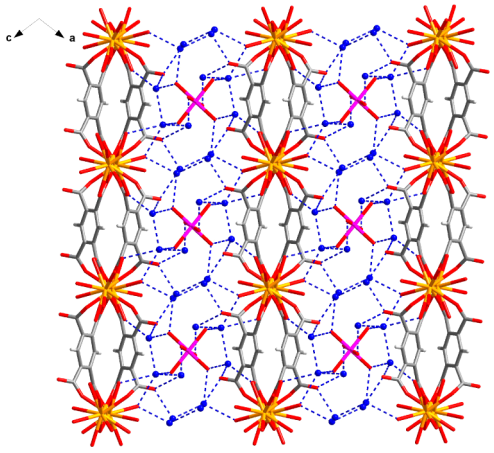

Figure 1. Projection along the crystallographic b-axis of the supramolecular three-dimensional structure of **1** and **2**. The blue circles represent the crystallization water molecules, whereas the hydrogen bonds are drawn as dashed lines.

Each crystallographically independent lanthanide(III) ion in **1** [Nd(III)] and **2** [Eu(III)] is ten-coordinate by eight carboxylate-oxygen atoms [O(1), O(2), O(2)$^{(a-1)}$, O(5)$^{(b-1)}$, O(7)$^{(c-1)}$, O(3)$^{(a-1)}$, O(8)$^{(c-1)}$, O(7)$^{(b-1)}$] from four different

dx.doi.org/10.1021/ic5008582 | Inorg. Chem. 2014, 53, 6299−6308

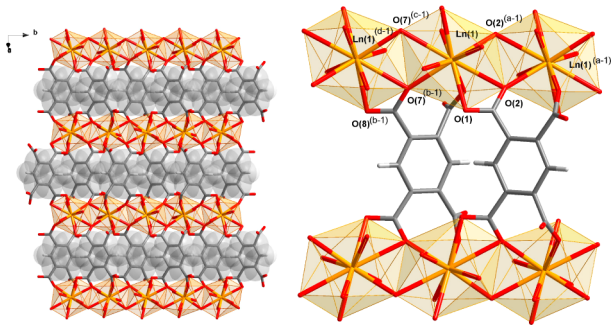

Figure 2. (Left) A view of a fragment of the anionic layer $[Ln(bta)(H_2O)_2]_n^{n-}$ [Ln = Nd (**1**) and Eu (**2**)] extended in the $(\bar{1}01)$ plane. (Right) Detail of the regular alternating bridging pathway in the chain of lanthanide(III) ions growing along the crystallographic *b*-axis.

bta^{4-} ligands, and two coordination water molecules [O(1w) and O(2w)] [see Figure 3 (**1**) and Figure S2 in the Supporting

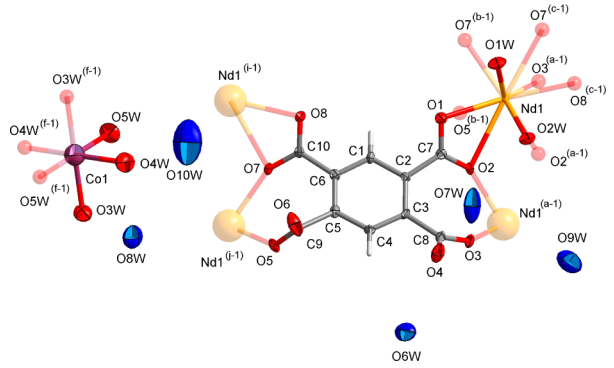

Figure 3. A perspective view of the asymmetric unit of **1** showing the atom numbering and the coordination modes of the bta ligand. The same atom numbering has been adopted for **2** (see Figure S1 in the Supporting Information).

Information (**2**)]. All these atoms build a distorted bicapped square antiprism with values of the bite parameter *b* equal to 0.98 (**1**) and 1.04 (**2**).[20] The Ln−O bond lengths vary in the ranges of 2.436(4)−2.713(4) Å (**1**) and 2.476(4)−2.709(4) Å (**2**) (see Table S2 in the Supporting Information). The base and upper planes of the polyhedron are built by the $O(1)O(2)^{(a-1)}O(5)^{(b-1)}O(2w)$ and $O(7)^{(c-1)}O(3)^{(a-1)}O(8)^{(c-1)}O(1w)$ sets of atoms respectively, with the O(2) and $O(7)^{(c-1)}$ atoms capping them (see Figure S2 in the Supporting Information). The values of the dihedral angle between the two square bases are 1.74(12)° (**1**) and 1.80(10)° (**2**). The largest Ln−O distances correspond to the bonds with the oxygen atoms capping the antiprism [mean values of 2.704(4) Å (**1**) and 2.706(4) Å (**2**)].

A clear decrease in the Ln−O carboxylate and Ln−O water bond distances has been observed with the increase in the atomic number of the lanthanide ion [see Figure S3 (left) in the Supporting Information]; this effect is closely related to the lanthanide contraction effect.[21]

Only one crystallographically independent cobalt(II) ion [Co(1)] occurs in **1** and **2**, which lies on a crystallographic inversion site [see Figure 3 (**1**) and Figure S1 in the Supporting Information (**2**)]. It is surrounded by six coordination water molecules in a slightly elongated octahedral environment [ϕ = 59.06 (**1**)/59.43° (**2**) and s/h = 1.23 (**1**)/1.23 (**2**) to be compared to the ideal values for octahedral environment, ϕ = 60° and s/h = 1.22][22] with O(4w), $O(4w)^{(f-1)}$, O(5w), and $O(5w)^{(f-1)}$ in equatorial positions and O(3w) and $O(3w)^{(f-1)}$ in the axial ones $[(f-1) = -x, 2-y, -z]$. The mean values of the equatorial Co−O water bond lengths are 2.082(6) Å (**1**) and 2.086(6) Å (**2**). They are somewhat shorter than the axial bond lengths [2.125(5) and 2.118(6) Å for **1** and **2**, respectively]. All these structural features agree with those previously reported for another hexaaquacobalt(II) unit in the ionic salt of formula $[Co(H_2O)_6](H_2bta)\cdot dpo\cdot 4H_2O$ (dpo = 4,4′-bipyridine-*N*,*N*′-dioxide).[12f] The six-coordinate cobalt(II) units are well-separated from each other, the values of the shortest interionic Co−Co distance being 8.710(3) Å (**1**) and 8.666(2) Å (**2**) $[Co(1)\cdots Co(1)^{(g-1)}; (g-1) = x, -1+y, z]$. These values are somewhat longer than the shortest cobalt−lanthanide separation [7.7208(5) Å (**1**) and 7.6793(14) Å (**2**) for $Co(II)\cdots Ln(III)^{(h-1)}; (h-1) = x, y, -1+z$].

The bta^{4-} ligand in **1** and **2** adopts a tetrakis-bidentate bridging mode through its four carboxylate groups subtending two four-membered [O(1) and O(2) toward Ln(1) and O(7) and O(8) toward $Ln(1)^{(j-1)}; (j-1) = -0.5+x, 0.5-y, -0.5+z$] and two seven-membered [O(2) and O(3) toward $Ln(1)^{(a-1)}$ and O(5) and O(7) toward $Ln(1)^{(k-1)}; (k-1) = 0.5-x, -0.5+y, -0.5-z$] chelate rings [see Figure 3 (**1**) and Figure S1 in the Supporting Information (**2**)]. The average values for the C−O distances of the tetracarboxylate ligand [1.258(5) Å (**1**) and 1.256(8) Å (**2**)] agree with those previously observed in other structurally characterized bta-containing metal complexes.[12,13] The whole bta^{4-} ligand is far from being planar, the values of the dihedral angle between the aromatic ring and the carboxylate groups being 38.1(2)°, 42.3(2)°, 43.8(2)°, and 77.5(2)° for **1** and 38.3(2)°, 42.2(2)°, 43.5(2)°, and 75.7(2)° for **2**. Finally, the internal angles in the benzene ring at the substituted C atoms [mean values of 118.8(6)° (**1**)/118.5(2)° (**2**)] are slightly smaller than those at the unsubstituted ones [122.4(6)° (**1**)/121.7(2)° (**2**)], in agreement with previous reports.[12,13]

*$[Ln_2Co(bta)_2(H_2O)_8]_n\cdot 6nH_2O$ [Ln = Eu(III) (**3**), Sm(III) (**4**), Gd(III) (**5**), and Tb(III) (**6**)].* The complexes **3**−**6** are isomorphous and their crystal structure is composed of neutral layers of the $[Ln_2Co(bta)_2(H_2O)_8]$ formula unit and crystallization water molecules that are interlinked by hydrogen bonds, leading to a supramolecular three-dimensional network (see Figure 4 and Table S3 in the Supporting Information). The layers are regularly stacked along the [110] direction, following an *ABAB* sequence. Within each layer, pairs of $[Ln(H_2O)_3]$ units with double oxo(carboxylate)- and double *syn*−*syn* carboxylate bridges occur, which, in turn, are connected by *trans*-diaquacobalt(II) entities along the crystallographic *c*-axis [Figure 5 (top)]. These heterobimetallic chains are cross-linked by the bta skeleton to afford the neutral layers [Figure 5 (bottom)]. The values of lanthanide−lanthanide separation and angle at the oxo(carboxylate) bridge are 3.9574(4) (**3**), 3.9853(2) (**4**), 3.9413(4) (**5**), and 3.9216(2) Å (**6**) $[Ln(1)\cdots Ln(1)^{(a-2)}; (a-2) = 1-x, 1-y, 2-z]$ and 106.39(1) (**3**), 106.53(1) (**4**), 106.47(1) (**5**), and 106.4(1)° (**6**) $[Ln(1)-O(1)-Ln(1)^{(a-2)}]$, whereas the shortest lanthanide−cobalt separations along the crystallographic *c*-axis are 5.3239(2) Å (**3**), 5.2219(3) Å (**4**), 5.3249(3) Å (**5**), and 5.3220(2) Å (**6**) $[Co(1)\cdots Ln(1)]$. These intrachain metal−metal distances are smaller than the shortest lanthanide−lanthanide [ranged from 9.1909(6) Å to 9.2186(8) Å] and Co−

dx.doi.org/10.1021/ic5008582 | *Inorg. Chem.* 2014, 53, 6299−6308

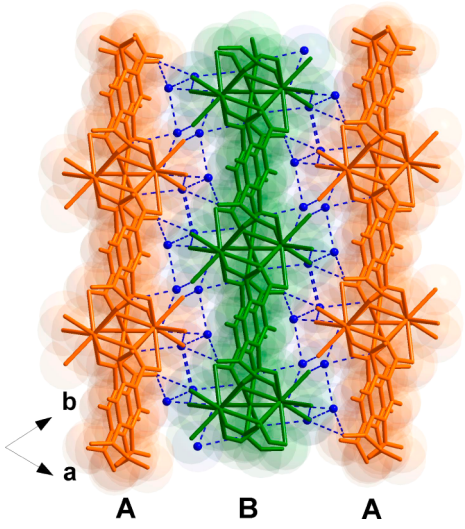

Figure 4. Projection along the crystallographic *c*-axis of the supramolecular three-dimensional structure of **3**–**6**, showing the *ABAB* stacking trend, together with the network of hydrogen bonds (blue dashed lines).

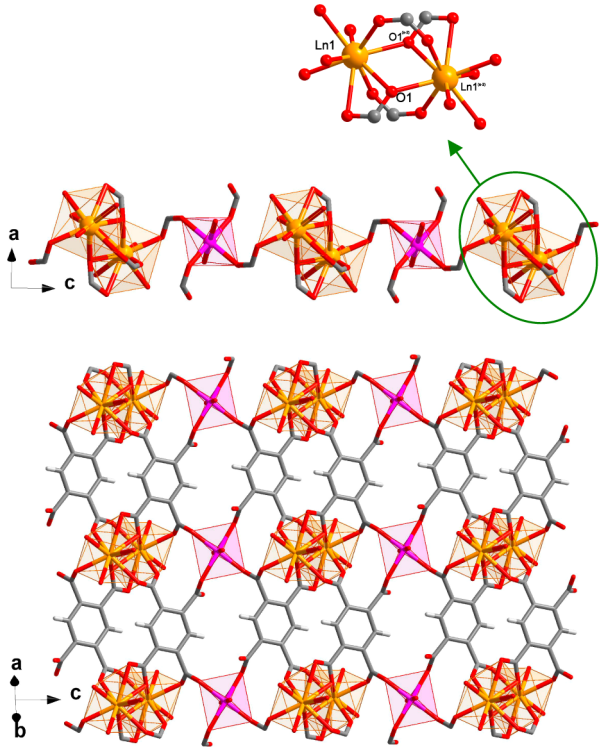

Figure 5. (Top) View of a fragment of the Co(II)–Ln(III) heterometallic chain running along the crystallographic *c*-axis. The inset shows a detail of the bridging pathway involving the lanthanide(III) dimers. (Bottom) Projection along the [110] direction of the layers of $[Ln_2Co(bta)_2(H_2O)_8]$ [Ln = Eu(III) (**3**), Sm(III) (**4**), Gd(III) (**5**), and Tb(III) (**6**)], showing how the heterometallic chains are linked through the skeleton of the bta ligand.

Co [values from 9.1909(5) Å to 9.2186(8) Å] separations across the bridging bta ligand.

Each crystallographically independent lanthanide(III) ion in **3**–**6** is nine-coordinate by six carboxylate oxygen atoms [O(1), $O(1)^{(a-2)}$, $O(2)^{(a-2)}$, O(3), $O(7)^{(b-2)}$, and $O(8)^{(c-2)}$; $(b-2) = 1+x, -1+y, z$ and $(c-2) = -x, 2-y, 2-z$] from four different bta^{4-} ligands and three water molecules [O(1w), O(2w), and O(3w)] [see Figure 6 (**4**) and Figure S3 in the

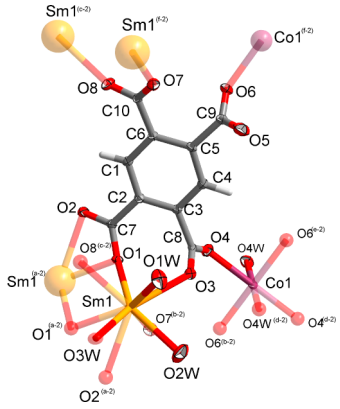

Figure 6. A perspective view of a fragment of the structure of **4** showing the coordination modes of the bta ligand, together with the atom numbering scheme. Thermal ellipsoids (drawn at 50% probability level) have been used to denote the crystallographically independent unit. The crystallization water molecules have been omitted for the sake of clarity.

Supporting Information (**3**, **5**, and **6**)]. This set of donor atoms builds a distorted monocapped square antiprism around the trivalent rare-earth cation [mean values for the *b* parameter equal to 1.01 (**3**), 1.18 (**4**), 1.01 (**5**), and 1.17 (**6**)].[20] The average values of the Ln–O bond lengths are 2.4760(2) (**3**), 2.4875(2) (**4**), 2.4653(3) (**5**), and 2.4585(5) (**6**) (see Table S4 in the Supporting Information). The square-planar base of the polyhedron is defined by the O(1), O(1w), O(3), and $O(8)^{(c-2)}$ atoms, while the upper square-plane is built by $O(1)^{(a-2)}$, $O(7)^{(b-2)}$, O(2w), and O(3w). The antiprism is capped by the $O(2)^{(a-2)}$ atom, with the corresponding Ln–O distance being the longest one [values that cover the range 2.663(2)–2.674(2) Å; see Table S3 in the Supporting Information] and contributing to the distortion of the polyhedron (see Figure S4 in the Supporting Information). The values of the Ln–O carboxylate bond distance are slightly shorter than those observed for the Ln–O water bond distance, and the mean values of the Ln–O carboxylate and Ln–O water bond lengths gradually decrease when going from Sm(III) to Tb(III) as expected due to the contraction of the ionic radii with the increasing atomic number of the 4f ions [see Figure S3 (right) and Table S4 in the Supporting Information].

Also, one crystallographically independent cobalt(II) ion [Co(1)] occurs in **3**–**6** (see Figure 6 and Figure S5 in the Supporting Information), which lies on a crystallographic inversion site. It is six-coordinate with four carboxylate oxygen atoms [O(4), $O(4)^{(d-2)}$, $O(6)^{(e-2)}$ and $O(6)^{(d-2)}$; symmetry code: $(d-2) = 1-x, 1-y, 1-z$; $(e-2) = -x, 2-y, 1-z$] from four different bta^{4-} ligands, and two coordination water molecules [O(4w) and $O(4w)^{(d-2)}$] describing a somewhat compressed octahedral environment [values of ϕ and s/h parameters of 60.31° and 1.21 (**3**), 60.26° and 1.21 (**4**), 60.27° and 1.21 (**5**) and 60.44° and 1.21 (**6**) versus the ideal values for an octahedral environment (60° and 1.22)].[22] The mean values of the equatorial Co–O bond length are 2.116(3) (**3**), 2.117(3) (**4**), 2.116(3) (**5**), and 2.123(3) Å (**6**); these values are somewhat longer than the axial bond lengths [2.090(3), 2.089(2), 2.087(3), and 2.084(3) Å for **3**, **4**, **5**, and **6**, respectively].

dx.doi.org/10.1021/ic5008582 | *Inorg. Chem.* 2014, 53, 6299–6308

Only one crystallographically independent bta^{4-} ligand is present in **3**–**6**. It adopts simultaneously tetrakis-monodentate [through O(4), O(6), O(7), and O(8) toward Co(1), $Co(1)^{(f-2)}$, $Ln(1)^{(f-2)}$, and $Ln(1)^{(c-2)}$, respectively; $(f - 2) = -1 + x, 1 + y, z$] and bis-bidentate coordination modes [through O(1) and O(2) toward $Ln(1)^{(a-2)}$ and via O(1) and O(3) toward Ln(1) subtending four- and seven-membered rings, respectively] (see Figure 6 and Figure S5 in the Supporting Information). The average values of the C–O bond distances in **3**–**6** [1.258(5) (**3**), 1.260(5) (**4**), 1.257(5) (**5**), and 1.259(1) Å (**6**)] agree with those observed in **1** and **2**. The values of the dihedral angles between the mean plane of the aromatic ring and the planes of the carboxylate groups vary in the ranges of 23.88(13)–87.49(14) (**3**), 24.2(2)–88.1(3) (**4**), 24.08(11)–87.15(13) (**5**), and 24.0(3)–87.0(4)° (**6**).

Magnetic Properties of 3–6. Because of the difficulties in the analysis and interpretation of the magnetic properties of mixed six-coordinate high-spin cobalt(II) and lanthanide(III) units, we would like to make some considerations prior to the presentation, analysis, and discussion of the magnetic data of **3**–**6**.

The different factors that challenge the analysis of the magnetic properties of the present mixed 3d–4f systems are the following:

(i) the first-order angular momentum of the six-coordinate high-spin cobalt(II) and the trivalent lanthanide ion (with the exception of the Gd^{3+}), which prevent the use of the spin-only formalism;

(ii) the value of the crystal field splitting of the rare-earth cation, which is usually on the order of kT at room temperature and, so, the thermal population of the Stark levels must be implicitly taken into account;

(iii) the inner nature of the 4f orbitals, with respect to the 3d ones, which is responsible for the weak magnetic interactions observed in 3d–4f systems and whose nature and magnitude can be obscured by the orbital contributions, crystal field effects, and intermolecular interactions.

In this respect, the very low efficiency of the extended bta ligand to mediate magnetic interactions between paramagnetic centers in bta-bridged systems in the temperature range studied,[12,10] allow us to conclude that the only possible exchange pathways involved in **3**–**6** concern the single *anti–syn* carboxylate bridge between Co(II) and Ln(III) and the double oxo(carboxylate) and double *syn–syn* carboxylate bridges between the lanthanide(III) cations within the heterobimetallic chains along the crystallographic *c*-axis [see Figure 5 (top)]. As far as we are aware, magneto-structural reports dealing with the first exchange pathway have not offered a straightforward conclusion about the occurrence of a significant magnetic interaction[23] whereas for the second one, weak antiferromagnetic interactions are documented for the digadolinium(III) pair [$-J$ values covering the range of 0.022–0.43 cm^{-1} through the Hamiltonian $\hat{H} = -J\hat{S}_1 \cdot \hat{S}_2$][24] and lack of magnetic coupling for the diterbium(III) couple.[25]

The magnetic properties of compounds **3**–**6**, under the form of the $\chi_M T$ product vs T plots [χ_M being the magnetic susceptibility per $Ln^{III}_2Co^{II}$ unit] are shown in Figures 7 (**3**), 8 (**4**), 9 (**5**), and 10 (**6**), whereas those of the magnetization versus H plot at 2.0 K are depicted in Figure S6 in the Supporting Information (**3**–**6**). The profiles of Figures 7–10 are similar to a continuous decrease of $\chi_M T$ upon cooling.

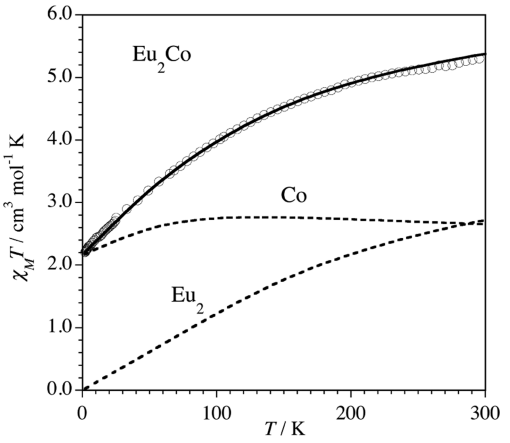

Figure 7. $\chi_M T$ vs T plot for **3**: (○) experimental and (—) best-fit curve. The dashed lines correspond to the theoretical curves for a Co(II) (middle) and two Eu(III) ions (bottom) calculated from the best-fit parameters (see text).

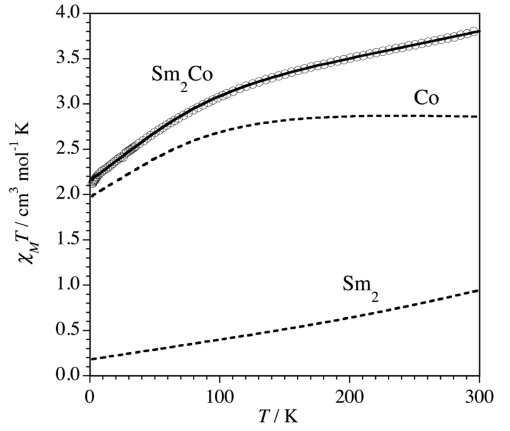

Figure 8. $\chi_M T$ vs T plot for **4**: (○) experimental and (—) best-fit curve. The dashed lines correspond to the theoretical curves for a Co(II) (middle) and two Sm(III) ions (bottom) calculated from the best-fit parameters (see text).

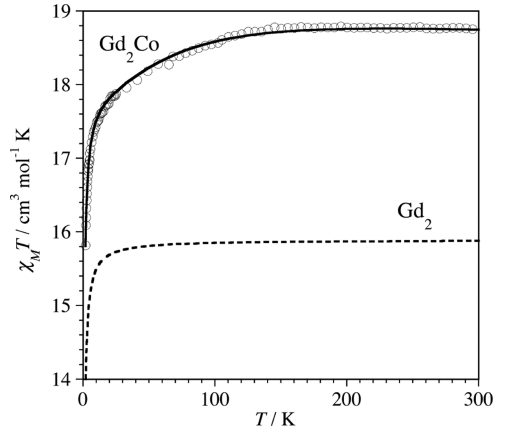

Figure 9. $\chi_M T$ vs T plot for **5**: (○) experimental; (–) best-fit curve. The dashed line corresponds to the theoretical curve for two Gd(III) ions magnetically interacting with $J_{GdGd} = -0.035$ cm^{-1} (see text).

Hereafter, we will proceed to analyze and discuss these plots in a separate manner for pedagogical reasons.

At room temperature, $\chi_M T$ for **3** is equal to 5.37 cm^3 mol^{-1} K. Upon cooling, $\chi_M T$ monotonically decreases to reach a value

dx.doi.org/10.1021/ic5008582 | Inorg. Chem. 2014, 53, 6299–6308

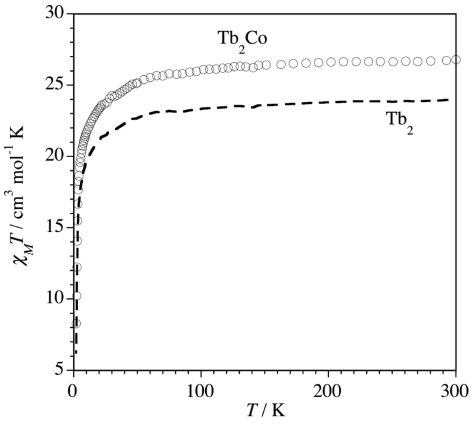

Figure 10. $\chi_M T$ vs T plot for **6**. The dashed line corresponds to the magnetic behavior of the two Tb(III) ions in **6** [the corresponding $\chi_M T$ curve for the Co(II) ion has been subtracted from the experimental one] (see text).

of 2.20 cm^3 mol^{-1} K at 2.0 K (Figure 7). The interpretation of the magnetic behavior of **3** is quite straightforward. In fact, although the ground state ($^7F_0$) for the Eu(III) is nonmagnetic ($4f^6$, $J = 0$, $S = 3$ and $L = 3$), the $^7F_1$ and $^7F_2$ excited states are sufficiently close to the lowest $^7F_0$ state to be populated at room temperature. This feature and the unquenched orbital contribution of the high-spin Co(II) ion would account for the magnitude of $\chi_M T$ per $Eu^{III}_2Co^{II}$ unit of **3** at 300 K. The observed decrease of $\chi_M T$ in the high-temperature domain is due the thermal depopulation of these excited states and the spin−orbit coupling effects of the high-spin Co(II) ion. Given that only the nonmagnetic $^7F_0$ ground state is populated at very low temperatures, the magnetically isolated Co(II) ion would be responsible for the magnetic data in this domain. Consequently, the magnetic data of **3** were analyzed through the Hamiltonian [eqs 1−4].

$$\hat{H} = \hat{H}_{SO} + \hat{H}_{Axial} + \hat{H}_{Zeeman} \quad (1)$$

$$\hat{H}_{SO} = \alpha\lambda\hat{L}_{Co}\hat{S}_{Co} - \lambda_{Ln}(\hat{L}_{Ln1}\hat{S}_{Ln1} + \hat{L}_{Ln2}\hat{S}_{Ln2}) \quad (2)$$

$$\hat{H}_{Axial} = \Delta(\hat{L}^2_{z,Co} - 2/3) \quad (3)$$

$$\hat{H}_{Zeeman} = \beta H(-\alpha\hat{L}_{Co} + 2\hat{S}_{Co} + \hat{L}_{Ln1} + 2\hat{S}_{Ln1} + \hat{L}_{Ln2} + 2\hat{S}_{Ln2}) \quad (4)$$

The first term in eq 1 accounts for the spin−orbit coupling effects, the second one corresponds to the axial distortion of the Co(II) ion, and the third one is the Zeeman interaction. $L = 1$ (P-isomorphism)[26] and $S = 3/2$ for Co(II) and $L = 3$ and $S = 3$ for Ln1 = Ln2 = Eu(III). α is defined as $\alpha = A\kappa$, with A being a parameter whose value depends on the strength of the crystal field [its value varies between 3/2 (weak crystal field) and 1 (strong crystal field)][26] and κ being the orbital reduction factor. λ_{Co} and λ_{Ln} are the spin−orbit coupling parameters of the Co(II) and Eu(III) ions, respectively, and Δ is the energy gap between the singlet $^4A_{2g}$ and doublet ^4E_g levels issued from the splitting of the orbital triplet $^4T_{1g}$ ground state under an axial distortion (see Figure 11). Best-fit parameters through matrix diagonalization techniques by using the VMPAG program[27] are $\alpha = 1.29(1)$, $\Delta = -1860(20)$ cm^{-1}, $\lambda_{Co} = -110(2)$ cm^{-1}, and $\lambda_{Eu} = +340(3)$ cm^{-1}. The theoretical curve reproduces well the experimental data in the entire temperature range explored.

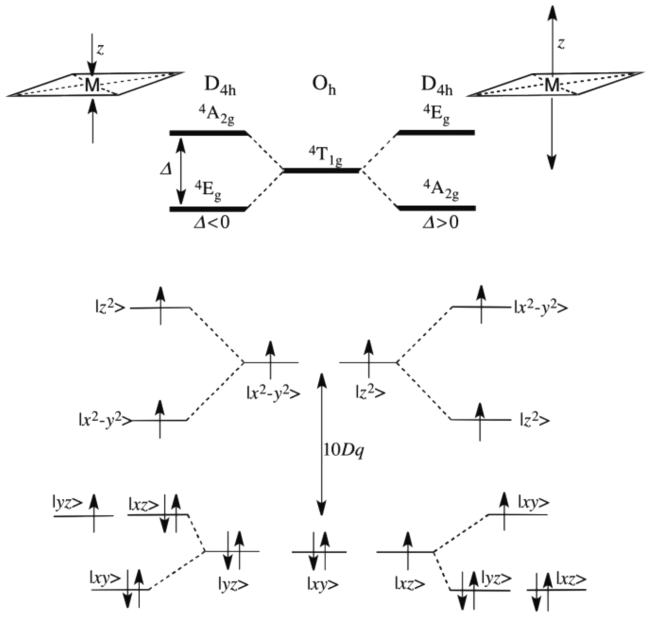

Figure 11. (Top) Splitting of the $^4T_{1g}$ term of a six-coordinated Co(II) ion in O_h symmetry (middle) and under axial (D_{4h}) compression (left) and elongation (right). (Bottom) The corresponding electronic configurations of the d orbitals (see text).

The value of λ_{Eu} agrees with those in the literature[28] and those of $\kappa = 0.85$ (calculated by assuming $A = 3/2$) and λ_{Co} are within the range of those reported for octahedral Co(II) ions surrounded by six oxygen atoms.[29] Finally, the negative value of Δ indicates that the orbital doublet ^4E_g is the ground level for the octahedrally compressed Co(II) ion (D_{4h} symmetry) in **3**, as shown in Figure 11. Although the sign of Δ is difficult to determine by the fit of the magnetic data of polycrystalline samples, in the present case, this sign is strongly supported by the fact that the value of $\chi_M T$ at 2.0 K for **3** is 2.20 cm^3 mol^{-1} K, which is a value that can only be attained for magnetically isolated six-coordinate Co(II) ions with negative values of Δ below -1600 cm^{-1}.[30] For positive Δ values (elongated octahedron), the value of $\chi_M T$ at low temperature tends to 1.7−1.8 cm^3 mol^{-1} K.[30]

In order to visualize the magnetic behavior of such unusual octahedrally compressed Co(II) ion as well as the corresponding one for Eu(III), the theoretical $\chi_M T$ curves for a Co(II) (middle dashed line) and two magnetically isolated Eu(III) ions (bottom dashed line), calculated by using the above determined best-fit parameters, are included in Figure 7.

At room temperature, $\chi_M T$ for **4** is equal to 3.80 cm^3 mol^{-1} K (Figure 8). This value is somewhat above that which is expected for a magnetically noninteracting six-coordinate high-spin Co(II) ion with an unquenched angular momentum (values of $\chi_M T$ varying in the range of 3.4−2.7 cm^3 mol^{-1} K)[30] plus two magnetically isolated Sm(III) centers [$\chi_M T$ per Sm(III) equal to 0.09 cm^3 mol^{-1} K for the $^6H_{5/2}$ low-lying state ($4f^5$, $J = 5/2$, $L = 5$, $g_J = 2/7$, and $S = 5/2$)]. As the ^6H ground state for Sm(III) is split into six levels by the spin−orbit coupling, the energies increasing from $^6H_{5/2}$ to $^6H_{15/2}$, the first excited state ($^6H_{7/2}$) would be populated at room temperature [λ for the Sm(III) ion is ca. 200 cm^{-1}],[31] this feature accounting for this greater value of $\chi_M T$ for **3**. Upon cooling, $\chi_M T$ continuously decreases to reach a value of 2.12 cm^3 mol^{-1} K at 2.0 K. The decrease of $\chi_M T$ in the high-temperature

dx.doi.org/10.1021/ic5008582 | Inorg. Chem. 2014, 53, 6299−6308

domain is due to spin−orbit coupling and crystal-field effects of the Co(II) and Sm(III) ions.

Because of the extremely weak spin density on the Sm(III) ion at low temperatures [$\chi_M T$ per one Sm(III) at 2.0 K being ca. 0.09 cm^3 mol^{-1} K), the magnetic interactions in the Sm(III)−Sm(III) and Co(II)−Sm(III) would be negligible. This is supported by the M versus H plot at 2.0 K (see Figure S6 in the Supporting Information), where one can see how the magnetization data of the isostructural compounds **3** and **4** are practically superimposed upon each other, the value of the saturation magnetization corresponding to a magnetically isolated six-coordinate Co(II) ion.[29] Consequently, the magnetic susceptibility data of **4** were analyzed through the Hamiltonian of eqs 1−4 with $L = 1$ and $S = 3/2$ for Co(II) and $L = 5$ and $S = 5/2$ for Ln1 = Ln2 = Sm(III). Best-fit parameters obtained by matrix diagonalization techniques through the VMPAG program lead to the following set of parameters: $\alpha = 1.29(1)$, $\Delta = -1004(10)$ cm^{-1}, $\lambda_{Co} = -148(2)$ cm^{-1}, and $\lambda_{Sm} = +194(2)$ cm^{-1}. The theoretical curve matches well with the experimental data in the entire temperature range investigated. The value of λ_{Sm} agrees with those given in the literature.[9] The middle and bottom dashed lines in Figure 8 represent the theoretical $\chi_M T$ curves (using the above best-fit parameters) for an isolated Co(II) ion and two independent Sm(III) ions, respectively. The magnetic behavior for the Co(II) in **4** is similar to that shown for the Co(II) ion in the isostructural europium(III) derivative (**3**).

$\chi_M T$ for **5** at 300 K is equal to 18.82 cm^3 mol^{-1} K, a value which is as expected for a magnetically isolated high-spin Co(II) ion with an important orbital contribution plus two magnetically noninteracting gadolinium(III) ions [$\chi_M T = 15.75$ cm^3 mol^{-1} K per two Gd(III) ions with $S_{Gd} = 7/2$ and $g_{Gd} = 2.0$]. Each Gd(III) ion has a $^8S_{7/2}$ ground state ($4f^7$, $J = 7/2$, $L = 0$ and $S = 7/2$, and $g_{Gd} = 2.0$) being located at some 10^4 cm^{-1} below the first excited state. Upon cooling, $\chi_M T$ follows a Curie law until 140 K and further monotonically decreases to reach 15.80 cm^3 mol^{-1} K at 2.0 K (Figure 9). Spin−orbit coupling effects of the six-coordinate high-spin Co(II) ion together with weak antiferromagnetic interactions between the Gd(III) ions through double oxo(carboxylate) and double *syn*−*syn* carboxylate bridges would account for the observed decrease of $\chi_M T$. In this respect, an antiferromagnetic coupling (J) close to −0.04 cm^{-1} through this pathway is predicted according to the literature.[24]

Having this in mind, the magnetic data of **5** were treated through the Hamiltonian of eqs 5−9.

$$\hat{H} = \hat{H}_{SO} + \hat{H}_{Axial} + \hat{H}_{Exchange} + \hat{H}_{Zeeman} \quad (5)$$

$$\hat{H}_{SO} = \alpha\lambda\hat{L}_{Co}\hat{S}_{Co} \quad (6)$$

$$\hat{H}_{Axial} = \Delta(\hat{L}^2_{z,Co} - 2/3) \quad (7)$$

$$\hat{H}_{Exchange} = -J\hat{S}_{Gd1}\hat{S}_{Gd2} \quad (8)$$

$$\hat{H}_{Zeeman} = \beta H(-\alpha\hat{L}_{Co} + 2\hat{S}_{Co} + g_{Gd1}\hat{S}_{Gd1} + g_{Gd2}\hat{S}_{Gd2}) \quad (9)$$

The first and second terms in eq 5 account for the spin-obit coupling effects and axial distortion of Co(II) ion, the third one concerns the isotropic exchange (J_{GdGd} is the exchange coupling parameter), and the last one is the Zeeman interaction. Best-fit parameters are $\alpha = 1.28(1)$, $\Delta = -1100(11)$ cm^{-1}, $\lambda_{Co} = -130(2)$ cm^{-1}, $J_{GdGd} = -0.035(1)$ cm^{-1}, and $g_{Gd} = 2.00(1)$. A good match between the theoretical curve and the magnetic data is obtained over the entire temperature range investigated.

The magnetization for **5** at 5 T (the maximum available field in our magnetometer) is 16.20 μ_B (see Figure S6 in the Supporting Information), a value that is quite close to the saturation magnetization and that would correspond to a set of two Gd(III) ions and a six-coordinate Co(II) ion. The theoretical curve for a pair of Gd(III) ions magnetically interacting with $g_{Gd} = 2.0$ and $J_{GdGd} = -0.035$ cm^{-1} is shown as a dashed line in Figure 9, while the theoretical curve for an isolated Co(II) ion (using the above best-fit parameters) is shown in Figure S7 in the Supporting Information.

$\chi_M T$ for **6** at 300 K is equal to 27 cm^3 mol^{-1} K (Figure 10). This value is as expected for a magnetically isolated six-coordinate high-spin Co(II) ion with an important orbital contribution plus two magnetically noninteracting Tb(III) ions [$\chi_M T = 11.81$ cm^3 mol^{-1} K per one Tb(III) ion, with a $^7F_6$ low-lying state ($4f^8$, $J = 6$, $L = 3$, $g_J = 3/2$, and $S = 3$)]. Upon cooling, $\chi_M T$ smoothly decreases until 50 K and it further exhibits an abrupt decrease to reach 8.30 cm^3 mol^{-1} K at 2.0 K. The M vs H plot for **6** at 2.0 K (see Figure S6 in the Supporting Information) is far from reaching the saturation and the magnetization attains a value of 11.80 μ_B at 5 T. The decrease of $\chi_M T$ in **6** is governed by the spin−orbit coupling effects of the six-coordinate Co(II) ion plus the thermal depopulation of the Stark levels of the Tb(III) ion. Unfortunately, the overparameterization produced by introducing the crystal field parameters for Tb(III) precludes an unambiguous determination of the magnetic parameters.

However, assuming that the magnetic contribution of the octahedrally compressed Co(II) ion in **6** is equal to that estimated for this cation in **5**, and by subtracting the corresponding $\chi_M T$ curve to the experimental one, it is possible to visualize the corresponding $\chi_M T$ curve of the diterbium(III) pair in **6**. The dashed line in Figure 10 corresponds to this plot. One can see therein that the low value of $\chi_M T$ at 2.0 K [ca. 2.65 cm^3 mol^{-1} K for each Tb(III) ion] unambiguously supports the occurrence of a weak antiferromagnetic coupling between the Tb(III) ions through the double oxo(carboxylate) and double *syn*−*syn* carboxylate bridges.

CONCLUSION

The six new complexes presented here add new examples to the scarce list of the 3d−4f heteronuclear coordination polymers built up from polycarboxylate ligands. The preparation of these heterometallic systems is not an easy task, and serendipity sometimes plays a key role in obtaining new compounds. The use of the bta ligand with its high coordination ability can efficiently bind the lanthanide ions and act as a bridge between them or toward 3d metal ions. However, the unpredictability in the preparation of these systems is reflected in the different crystal structures of complexes **1** and **2** and **3**−**6**; it is also reflected by the fact that only the syntheses with Eu(III), Sm(III), Gd(III), and Tb(III) yielded heterometallic coordination polymers.

Despite the synthetic issues, the crystal structures support the trend of the lanthanide atoms to form dinuclear entities. The presence of a compressed six-coordinated Co(II) ion in **3**−**6** allowed us to carry out a thorough analysis of its magnetic behavior, as well as analyze the efficiency of the double oxo(carboxylate) and double *syn*−*syn* carboxylate bridges as exchange pathways for some trivalent lanthanide ions.

dx.doi.org/10.1021/ic5008582 | Inorg. Chem. 2014, 53, 6299−6308

■ ASSOCIATED CONTENT

Supporting Information

X-ray crystallographic data in CIF format; the selected intermolecular contacts for **1**−**6**; the figures of the crystallographically independent units with the numbering scheme of complexes **2**, **3**, **5** and **6**; the selected bond lengths and angles for compounds **1**−**6**; the lanthanide environments for compounds **1**−**6**; the variation of the average values of the $Ln-O_{carboxylate}$ and $Ln-O_{water}$ bond lengths, as a function of the atomic number; magnetization vs *H* plot at 2.0 K for $Ln(III)_2Co(II)$ [Ln = Eu (**3**), Sm (**4**), Gd (**5**), and Tb (**6**)]; and the theoretical curve for the Co(II) ion for compound **5**. This material is available free of charge via the Internet at http://pubs.acs.org.

■ AUTHOR INFORMATION

Corresponding Authors

*E-mail: fabelo@ill.fr (O. Fabelo).

*E-mail: caruiz@ull.edu.es (C. Ruiz-Pérez).

Notes

The authors declare no competing financial interest.

■ ACKNOWLEDGMENTS

Financial support from the Spanish Ministerio de Economía y Competitividad (MINECO) (through projects MAT2010-16981, CTQ2010-15364, MAT2011-2599, MAT2011-27233-C02-02), the Consolider-Ingenio (CSD2006-00015 "La Factoría" and CSD2007-00010), and the Generalitat Valenciana (through project ISIC2012/002) are gratefully acknowledged. P.D.-G. also thanks MINECO for predoctoral contracts through the FPI program. J.P. also thanks the Consolider-Ingenio for a postdoctoral contract (CSD2006-00015). The authors thank the Spanish BM16-beamline staff for its support.

■ REFERENCES

(1) (a) Ferey, G. *Chem. Soc. Rev.* **2008**, *37*, 191−214. (b) Kitagawa, S.; Kitaura, R.; Noro, S. *Angew. Chem., Int. Ed.* **2004**, *43*, 2334−2375. (c) Janiak, C. *Dalton Trans.* **2000**, *21*, 3885−3896. (d) Li, H.; Eddaoudi, M.; O'keeffe, M.; Yaghi, O. M. *Nature* **1999**, *402*, 276−279. (e) Batten, S. R.; Robson, R. *Angew. Chem., Int. Ed.* **1998**, *37*, 1460−1494. (f) Yaghi, O. M.; Li, H. L.; Davis, C. *Acc. Chem. Res.* **1998**, *31*, 474−484.

(2) (a) Stroppa, A.; Prashant, J.; Paolo, B.; Martijn, M.; Perez-Mato, J. M.; Anthony, K. C.; Harold, W. K.; Silvia, P. *Angew. Chem., Int. Ed.* **2011**, *50*, 5847−5850. (b) Eddaoudi, M.; Kim, J.; Rosi, N.; Vodak, D.; Wachter, J.; O'Keeffe, M.; Yaghi, O. M. *Science* **2002**, *295*, 469−472. (c) Janiak, C. *Dalton Trans.* **2003**, *14*, 2781−2804. (d) Dybtsev, D. N.; Nuzhdin, A. L.; Chun, H.; Bryliakov, K. P.; Talsi, E. P.; Fedin, V. P.; Kim, K. *Angew. Chem., Int. Ed.* **2006**, *45*, 916−920.

(3) (a) O'Keeffe, M.; Yaghi, O. M. *Chem. Rev.* **2012**, *112*, 675−702. (b) Kurmoo, M. *Chem. Soc. Rev.* **2009**, *38*, 1353−1379. (c) Allendorf, M. D.; Bauer, C. A.; Bhakta, R. K.; Houk, R. J. T. *Chem. Soc. Rev.* **2009**, *38*, 1330−1352. (d) Lee, J. Y.; Farha, O. K.; Roberts, J.; Scheidt, K. A.; Nguyen, S. T.; Hupp, J. T. *Chem. Soc. Rev.* **2009**, *38*, 1450−1459. (f) Sharples, J. W.; Collison, D. *Coord. Chem. Rev.* **2014**, *260*, 1−20.

(4) Kurmoo, M. *Chem. Soc. Rev.* **2009**, *38*, 1353−1379.

(5) (a) Andruh, M.; Costes, J.-P.; Díaz, C.; Gao, S. *Inorg. Chem.* **2009**, *48*, 3342−3359. (b) Wojciechowski, W.; Legendziewicz, J.; Puchalska, M.; Ciunik, Z. *J. Alloys Compd.* **2004**, *380*, 285−295. (c) Fabelo, O.; Cañadillas-Delgado, L.; Pasán, J.; Díaz-Gallifa, P.; Labrador, A.; Ruiz-Pérez, C. *CrystEngComm* **2012**, *14*, 765−767. (d) Sutter, J. P.; Kahn, M. L.; Golhen, S.; Ouahab, L.; Kahn, O. *Chem.—Eur. J.* **1998**, *4*, 571−576.

(6) (a) Zhao, B.; Cheng, P.; Dai, Y.; Cheng, C.; Liao, D.-Z.; Yan, S.-P.; Jiang, Z.-H.; Wang, G.-L. *Angew. Chem., Int. Ed.* **2003**, *42*, 934−936. (b) Osa, S.; Kido, T.; Matsumoto, N.; Re, N.; Pochaba, A.; Mrozinski, J. *J. Am. Chem. Soc.* **2004**, *126*, 420−421. (c) Mishra, A.; Wernsdorfer, W.; Abboud, K. A.; Christou, G. *J. Am. Chem. Soc.* **2004**, *126*, 15648−15649. (d) Mori, F.; Nyui, T.; Ishida, T.; Nogami, T.; Choi, K. Y.; Nojiri, H. *J. Am. Chem. Soc.* **2006**, *128*, 1440−1441. (e) Ako, A. M.; Hewitt, I. J.; Mereacre, V.; Cleťac, R.; Wernsdorfer, W.; Anson, C. E.; Powell, A. K. *Angew. Chem., Int. Ed.* **2006**, *45*, 4926−4929. (f) Bogani, L.; Wernsdorfer, W. *Nat. Mater.* **2008**, *7*, 179−186. (g) Novitchi, G.; Wernsdorfer, W.; Chibotaru, L. F.; Costes, J. P.; Anson, C. E.; Powell, A. K. *Angew. Chem., Int. Ed.* **2009**, *48*, 1614−1619. (h) Costes, J. P.; Dahan, F.; Dupuis, A. *Inorg. Chem.* **2000**, *39*, 165−168. (i) Costes, J. P.; Dahan, F.; Dupuis, A.; Laurent, J. P. *Inorg. Chem.* **1997**, *36*, 3429−3433.

(7) (a) He, F.; Tong, M.-L.; Yu, X.-L.; Chen, X.-M. *Inorg. Chem.* **2005**, *44*, 559−565. (b) Yan, Z.; Feng, L.; Song, Y.-M.; Feng, X.-F.; Luo, M.-B.; Liao, Z.-W.; Sun, G.-M.; Tian, X.-Z.; Yuan, Z.-J. *Cryst. Growth. Des.* **2012**, *12*, 2158−2161.

(8) (a) Bencini, A.; Benelli, C.; Caneschi, A.; Carlin, R. L.; Dei, A.; Gatteschi, D. *J. Am. Chem. Soc.* **1985**, *107*, 8128−8136. (b) Bencini, A.; Benelli, C.; Caneschi, A.; Dei, A.; Gatteschi, D. *Inorg. Chem.* **1986**, *25*, 572−575. (c) Benelli, C.; Caneschi, A.; Gatteschi, D.; Guillou, O.; Pardi, L. *Inorg. Chem.* **1990**, *29*, 1750−1755. (c) Andruh, M.; Ramade, I.; Codjovi, E.; Guillou, O.; Kahn, O.; Trombe, J. C. *J. Am. Chem. Soc.* **1993**, *115*, 1822−1829. (d) Bencini, A.; Benelli, C.; Caneschi, A.; Dei, A.; Gatteschi, D. *Inorg. Chem.* **1986**, *25*, 572−575. (e) Costes, J. P.; Dahan, F.; Dupuis, A.; Laurent, J. P. *Inorg. Chem.* **1996**, *35*, 2400−2402. (f) Costes, J. P.; Dahan, F.; Dupuis, A.; Laurent, J. P. *Inorg. Chem.* **1997**, *36*, 3429.

(9) (a) Guillou, O.; Kahn, O.; Oushoorn, R. L.; Boubekeur, K.; Batail, P. *Inorg. Chim. Acta* **1992**, *119*, 198−200. (b) Benelli, C.; Fabretti, A. C.; Giusti, A. *J. Chem. Soc., Dalton Trans.* **1993**, 409−412. (c) Sanz, J. L.; Ruiz, R.; Gleizes, A.; Lloret, F.; Faus, J.; Julve, M.; Borrás-Almenar, J. J.; Journaux, Y. *Inorg. Chem.* **1996**, *35*, 7384−7393. (d) Sanada, T.; Suzuki, T.; Kaizaki, S. *J. Chem. Soc., Dalton Trans.* **1998**, 959−966. (e) Kahn, M. L.; Mathonière, C.; Kahn, O. *Inorg. Chem.* **1999**, *38*, 3692−3697. (f) Kahn, O. *Acc. Chem. Res.* **2000**, *33*, 647−657. (g) Kou, H. Z.; Zhou, B. C.; Gao, S.; Wang, R. J. *Angew. Chem., Int. Ed.* **2003**, *42*, 3288−3291.

(10) Díaz-Gallifa, P.; Fabelo, O.; Cañadillas-Delgado, L.; Pasán, J.; Labrador, A.; Lloret, F.; Julve, M.; Ruiz-Pérez, C. *Cryst. Growth. Des.* **2013**, *13*, 4735−4745.

(11) (a) Domínguez, S.; Torres, J.; Peuffo, F.; Mederos, A.; González-Platas, J.; Castiglioni, J.; Kremer, C. *J. Mol. Struct.* **2007**, *829*, 57−64. (b) Li, J.-X.; Du, Z.-X.; Huang, W.-P. *Z. Naturforsch. B* **2011**, *66*, 1029−1033. (c) Li, J.-X.; Du, Z.-X.; Zhu, B.-L.; An, H.-Q.; Dong, J.-X.; Hu, X.-J.; Huang, W.-P. *Inorg. Chem. Commun.* **2011**, *14*, 522−525.

(12) (a) Fabelo, O.; Cañadillas-Delgado, L.; Pasán, J.; Delgado, F. S.; Lloret, F.; Cano, J.; Julve, M.; Ruiz-Pérez, C. *Inorg. Chem.* **2009**, *48*, 11342−11351. (b) Fabelo, O.; Pasán, J.; Cañadillas-Delgado, L.; Delgado, F. S.; Yuste, C.; Lloret, F.; Julve, M.; Ruiz-Pérez, C. *CrystEngComm* **2009**, *11*, 2169−2179. (c) Fabelo, O.; Pasán, J.; Cañadillas-Delgado, L.; Delgado, F. S.; Labrador, A.; Lloret, F.; Julve, M.; Ruiz-Pérez, C. *Cryst. Growth Des.* **2008**, *8*, 3984−3992. (d) Fabelo, O.; Pasán, J.; Cañadillas-Delgado, L.; Delgado, F. S.; Lloret, F.; Julve, M.; Ruiz-Pérez, C. *Inorg. Chem.* **2008**, *47*, 8053−8061. (e) Fabelo, O.; Pasán, J.; Lloret, F.; Julve, M.; Ruiz-Pérez, C. *Inorg. Chem.* **2008**, *47*, 3568−3576. (f) Fabelo, O.; Pasán, J.; Lloret, F.; Julve, M.; Ruiz-Pérez, C. *CrystEngComm* **2007**, *9*, 815−827.

(13) Cañadillas-Delgado, L.; Fabelo, O.; Ruiz-Pérez, C.; Delgado, F. S.; Julve, M.; Hernández-Molina, M.; Laz, M. M.; Lorenzo-Luis, P. *Cryst. Growth Des.* **2006**, *6*, 87−93.

(14) Henisch, K. In *Crystal Growth in Gels*; The Pennsylvania State University Press: Pittsburgh, PA, 1970.

(15) Duisenberg, A. J. M.; Kroon-Batenburg, L. M. J.; Schreurs, A. M. M. *J. Appl. Crystallogr.* **2003**, *36*, 220−229.

(16) Otwinowski, Z. Minor, W. Processing of X-ray Diffraction Data Collected in Oscillation Mode. In *Macromolecular Crystallography, Part*

A; Carter, C. W., Jr., Sweet, R. M., Eds.; Methods in Enzymology, Vol. *276*; Academic Press: New York, 1997; pp 307−326.
(17) Sheldrick, G. M. *Acta Crystallogr., Sect. A: Found Crystallogr.* **2008**, *64*, 112122.
(18) Spek, A. L. *J. Appl. Crystallogr.* **2003**, *36*, 7−13.
(19) *DIAMOND 2.1d, Crystal Impact GbR, CRYSTAL IMPACT*; K. Brandenburg & H. Putz GbR: Bonn, Germany, 2000.
(20) Ribas Gispert, J. *Química de Coordinacion*; Ediciones Omega, S.A., 2000.
(21) Stiefel, E. I.; Brown, G. F. *Inorg. Chem.* **1972**, *11*, 434−436.
(22) (a) Aguilà, D.; Barrios, L. A.; Velasco, V.; Arnedo, L.; Aliaga-Alcalde, N.; Menelaou, M.; Teat, S. J.; Roubeau, O.; Luis, F.; Aromí, G. *Chem.—Eur. J.* **2013**, *19*, 5881−5891. (b) Hutchings, A.-J.; Habib, F.; Holmberg, R. J.; Korobkov, I.; Murugesu, M. *Inorg. Chem.* **2014**, *53*, 2102−2112.
(23) (a) Zhao, X. Q.; Cui, P.; Zhao, B.; Shi, W.; Cheng, P. *Dalton Trans.* **2011**, *40*, 805−819. (b) Rodriguez-Martín, Y.; Hernández-Molina, M.; Delgado, F. S.; Pasán, J.; Ruiz-Pérez, C.; Sanchíz, J.; Lloret, F.; Julve, M. *CrystEngComm* **2002**, *4*, 440−446. (c) Rodríguez-Martín, Y.; Hernández-Molina, M.; Delgado, F. S.; Pasán, J.; Ruiz-Pérez, C.; Sanchíz, J.; Lloret, F.; Julve, M. *CrystEngComm* **2002**, *4*, 522−535.
(24) (a) Cañadillas-Delgado, L.; Fabelo, O.; Pasán, J.; Delgado, F. S.; Lloret, F.; Julve, M.; Ruiz-Pérez, C. *Dalton Trans.* **2010**, *39*, 7286−7293. (b) Cañadillas-Delgado, L.; Fabelo, O.; Cano, J.; Pasán, J.; Delgado, F. S.; Lloret, F.; Julve, M.; Ruiz-Pérez, C. *CrystEngComm* **2009**, *11*, 2131−2142. (c) Cañadillas-Delgado, L. Fabelo, O. Ruiz-Pérez, C. Cano, J. *Magnetic Interactions in Oxo-carboxylate Bridged Gadolinium(III) Complexes*; Nova Science Publishers: New York, 2010.
(25) Barja, B.; Aramendia, P.; Baggio, R.; Garland, M. T.; Peña, O.; Perec, M. *Inorg. Chim. Acta* **2003**, *355*, 183−190.
(26) (a) Figgis, B. N.; Gerloch, M.; Mabbs, F. E.; Webb, G. A. *J. Chem. Soc. A* **1968**, 2084−2086. (b) Gerloch, M.; Quested, P. N. *J. Chem. Soc. A* **1971**, 3725−3729. (c) Herrera, J. M.; Bleuzen, A.; Dromzée, Y.; Julve, M.; Lloret, F.; Verdaguer, M. *Inorg. Chem.* **2003**, *42*, 7052−7059. (d) Sharma, A. K.; Lloret, F.; Mukherjee, R. *Inorg. Chem.* **2007**, *46*, 5128−5130.
(27) Cano, J. *VMPAG package*; University of Valencia, Spain, 2003.
(28) (a) Andruh, M.; Bakalbassis, E.; Kahn, O.; Trombe, J. C.; Porcher, P. *Inorg. Chem.* **1993**, *32*, 1616−1622. (b) Hernandez-Molina, M.; Lorenzo-Luis, P.; Ruiz-Pérez, C.; López, T.; Martin, I. R.; Anderson, K. M.; Orpen, A. G.; Bocanegra, E. H.; Lloret, F.; Julve, M. *J. Chem. Soc., Dalton Trans.* **2002**, 3462−3470.
(29) Fabelo, O.; Pasán, J.; Lloret, F.; Julve, M.; Ruiz-Pérez, C. *Inorg. Chem.* **2008**, *47*, 3568−3576.
(30) Lloret, F.; Julve, M.; Cano, J.; Ruiz-García, R.; Pardo, E. *Inorg. Chim. Acta* **2008**, *361*, 3432−3445.
(31) Kahn, O. *Molecular Magnetism*; VCH Publishers: New York, 1993; p 49.